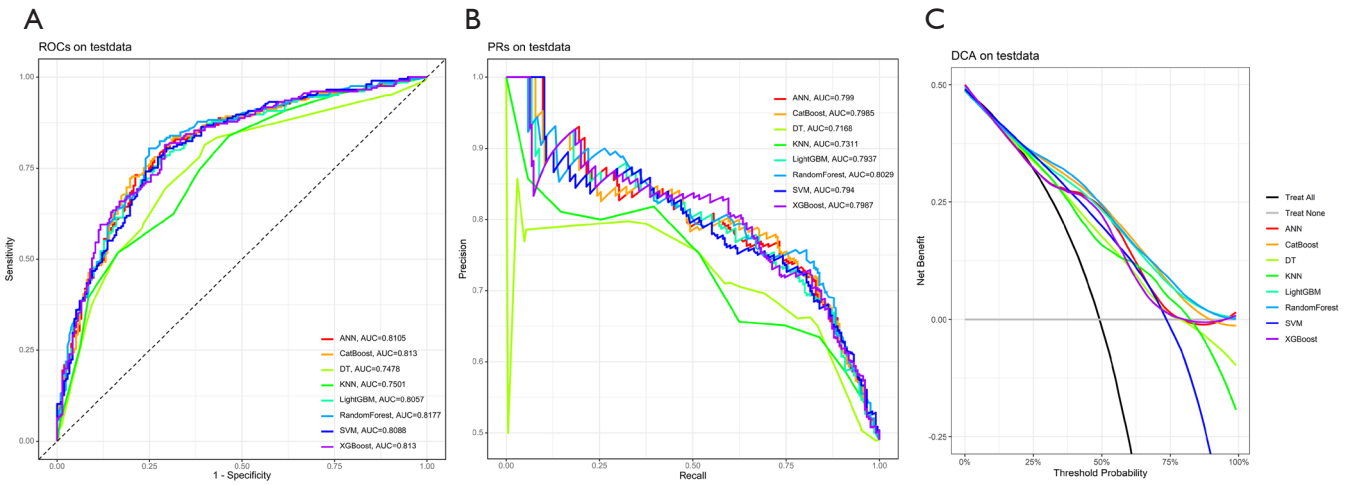

Figure S1 Predictive performance of the eight ML algorithms in the testing set. (A) ROC curves display the predictive model discrimination based on auROC scores. (B) PR curves display the predictive model discrimination based on auPR scores. (C) Decision curve analysis revealed the net benefit of the models in terms of clinical utility. ML, machine learning; ROC, receiver operating characteristic; PR, precision-recall curve.

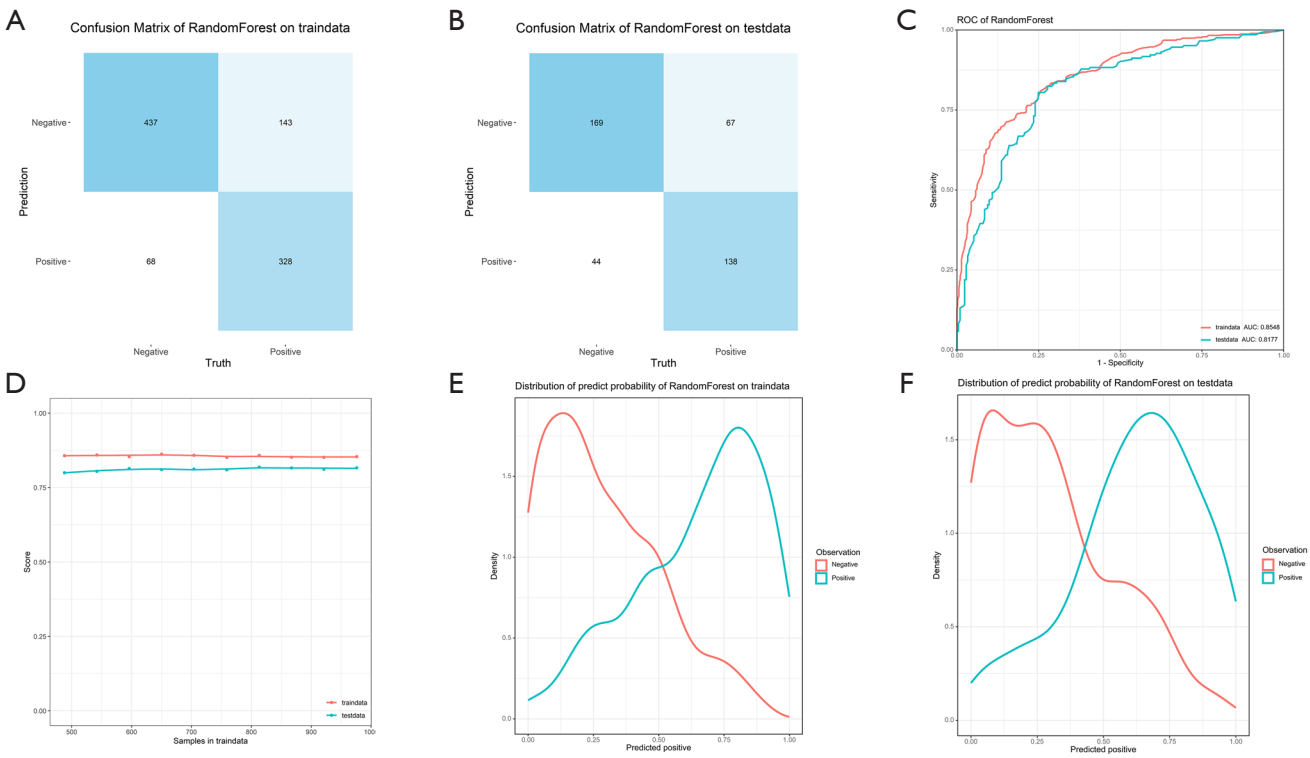

Figure S2 RF model performance. (A,B) Confusion matrix of the RF model. (C) ROC curves of the RF model in the training and testing cohorts. (D) Learning curves of the RF model. (E,F) Predicted probability distribution curves of the RF model. RF, random forest; ROC, receiver operating characteristic.

https://dx.doi.org/10.21037/gs-23-349

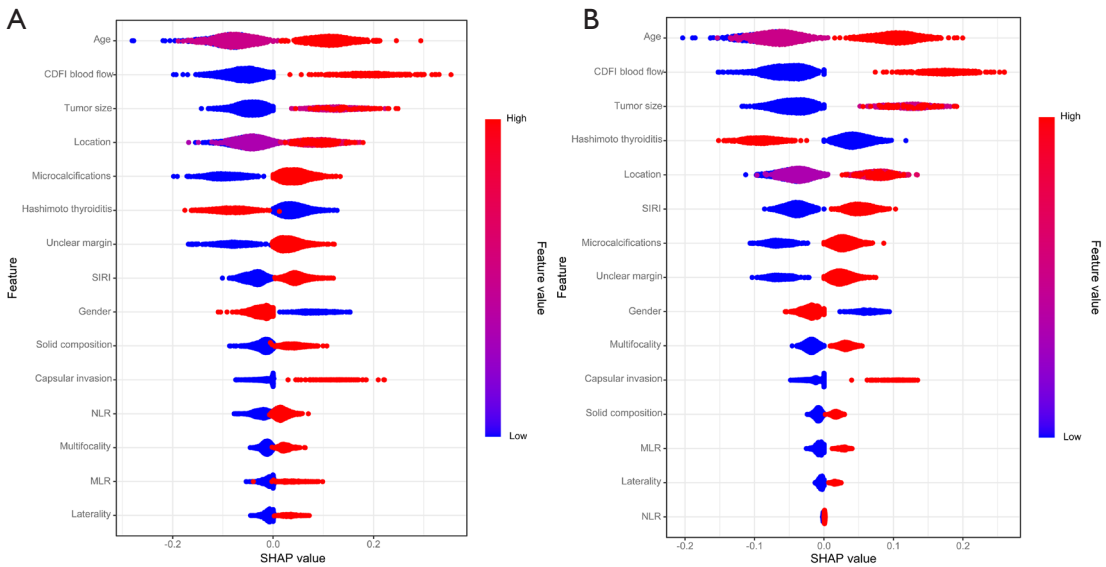

Figure S3 SHAP summary plot's scatter plot. (A) RF model; (B) XGBoost model. RF, random forest.

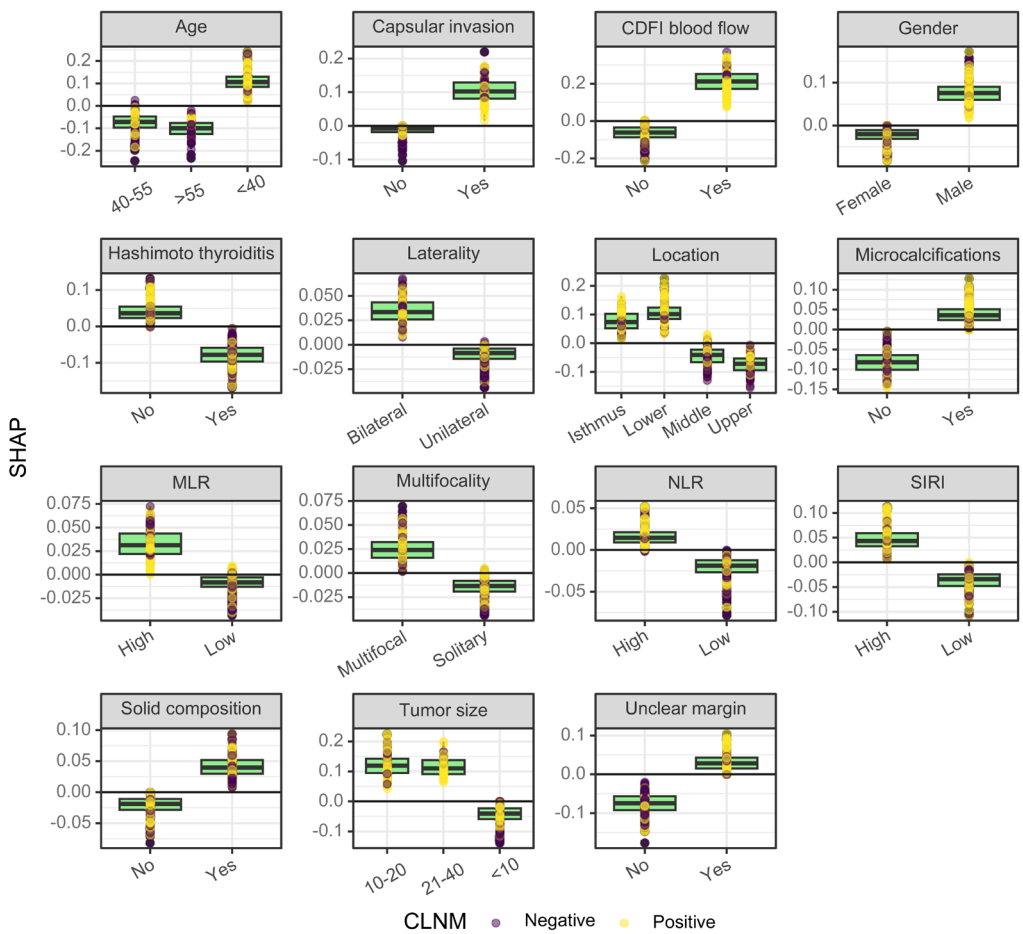

Figure S4 The facet wrap plot based on the SHAP value in the RF model. RF, random forest; CLNM, central lymph node metastasis; CDFI, color Doppler flow imaging; MLR, monocyte-to-lymphocyte ratio; NLR, neutrophil-to-lymphocyte ratio; SIRI, systemic inflammation response index.

https://dx.doi.org/10.21037/gs-23-349